European Polymer Journal 49 (2013) 923–931

Contents lists available at SciVerse ScienceDirect

European Polymer Journal

journal homepage: www.elsevier.com/locate/europolj

Structure and rheology of nanocomposite hydrogels composed of DNA and clay

Akihiro Taki, Baiju John, Shuichi Arakawa, Masami Okamoto *

Advanced Polymeric Nanostructured Materials Engineering, Graduate School of Engineering, Toyota Technological Institute, 2-12-1 Hisakata, Tempaku, Nagoya 468-8511, Japan

ARTICLE INFO

Article history:
Received 20 June 2012
Received in revised form 13 October 2012
Accepted 13 October 2012
Available online 23 October 2012

Keywords:
Nanocomposite hydrogels
DNA
Rheology
Stress relaxation

ABSTRACT

The preparation and characterization of the nanocomposite hydrogels based on deoxyribonucleic acid (DNA) and synthetic hectorite (SWN), were reported. Wide-Angle X-ray Diffraction (WAXD) and Fourier Transform Infrared Spectroscopy (FTIR) analyses confirmed that the intercalation of water molecules into the silicate galleries took place and the interaction between PO_2^- groups of DNA and SWN surfaces. DNA/SWN hydrogels exhibited viscoelastic solid-like properties DNA as revealed by rheological measurements. The stress-relaxation behaviors of DNA/SWN and SWN hydrogels in the linear viscoelastic regime and non-linear viscoelastic regime were examined. The incorporation of DNA macromolecules led to the enhancement of the damping behavior of the dispersed silicate particles as compared with SWN hydrogels without DNA. The softening of the nanocomposite hydrogels was supported by the calculated damping function of the stress-relaxation measurements.

1. Introduction

Over the last few years, the utility of inorganic nanoscale particles as filler to enhance the polymer performance has been established. Of particular interest is recently developed nanocomposite technology consisting of a polymer and organically modified layered filler (organo-clay) because they often exhibit remarkably improved mechanical and various other materials properties as compared with those of virgin polymer or conventional composite (micro/macro-composites) [1–6]. These concurrent property improvements are well beyond what can be generally achieved through the micro/macro-composites' preparation.

The synthetic strategy and molecular design was first explored by Toyota group with nylon 6 as the matrix polymer [7]. This new class of material is now being introduced in structural applications, such as gas barrier film and other load-bearing applications [5]. Polymer/clay nanocomposites (PCNs) and their self-assembly behaviors have recently been approached to produce nanoscale polymeric materials [1–6]. Additionally, these nanocomposites have been proposed as model systems to examine polymer structure and dynamics in confined environments [8–10].

The original mesoscale structure in PCNs consists of randomly oriented exfoliated clay layers or tactoids of layers. This randomly distributed nano-filler forms an "organo-clay network" structure, which is mediated by polymer chains and organo-clay interactions, responsible for the linear viscoelastic response observed in PCN melts. This meso-structure, which is intrinsically disordered metastable state and out-of-equilibrium, offers an apt analogy to soft colloidal glasses and gels [11,12].

Several kinds of inorganic clay particles have been introduced into polymer gel systems without additional use of chemical cross-linkers. Haraguchi et al. [13,14] reported that the properties of thermosensitive poly(*N*-isopropylacrylamide) (PNIPA)/synthetic hectorite hydrogels having the exfoliated clay particles, which act as multifunctional cross-links. The incorpolation of this clay markedly improves not only the mechanical and swelling–

* Corresponding author. Fax: +81 (0)52 809 1864.
E-mail address: okamoto@toyota-ti.ac.jp (M. Okamoto).

0014-3057/$ - see front matter © 2012 Elsevier Ltd. All rights reserved.
http://dx.doi.org/10.1016/j.eurpolymj.2012.10.013

deswelling properties but also the spatial homogeneity of the nanocomposite gels.

Apart from this, aqueous suspensions of clay are more or less flocculated and exhibit remarkable long-term gelation and yield stress thixotropic and rheopexy behavior as reported by van Olphen [15] some 30 years ago. In dilute suspensions of swelling clays such as hectorite and montmorillonite (MMT), the gelation takes place via a formation of a microflocculation due to electrostatic attraction between the positively charged edges and negatively charged faces of the plate-like particles, resulting in a card-house structure.

To broaden our knowledge on the key factors that control the mesoscale structure and properties of such hydrogels, we have characterized in this work deoxyribonucleic acid (DNA)/synthetic hectorite hydrogels prepared with different clay content. The DNA-based nanocomposite hydrogels will be worthwhile not only for assessing the dynamic properties under oscillatory shear and flow behavior, which are related to the mesoscale structure of the hydrogels but also for studying the interlayer confinement of the DNA molecules in bioinorganic nanostructued materials [16].

2. Experimental section

2.1. Materials

Synthetic hectorite consists of an octahedral $AlO_4(OH)_2$ sheet sandwiched between two SiO_4 tetrahedral layers (of ~1 nm thick and ~50 nm diameter) with the charges being adjusted by substituting Al^{3+} or Si^{4+} with Mg^{2+} and/or Li^+ and the depressed charges being neutralized with alkaline cations intercalated into the interlayer spaces to form a laminate structure of several layers. The chemical formula was $Na_{0.66}(Mg_{5.34}Li_{0.66})Si_8O_{20}(OH)_4$ having cation exchange capacity of 86.6 meq/100 g (as reported by the supplier, CO-OP Chemical Co. Ltd., Japan). The synthetic hectorite was designated as SWN. DNA, sodium salt from salmon testes was purchased from Sigma–Aldrich (D1626). The Guanine–Cytosine(G–C) content was reported to be 41.2%. The melting temperature was 87.5 °C in 0.15 M sodium chloride and 0.015 M sodium citrate. The molecular weight was 1.3×10^6 g/mol possessing ca. 2000 base pair.

DNA/SWN nanocomposite hydrogels (each containing 2.0 wt% DNA) with various concentrations of 4.0–22.0 wt% (volume fraction $\phi_{SWN} = 0.016–0.101$) were prepared by stirring at room temperature and equilibrates for 24 h to obtain transparent gels. Milli-Q ultrapure water was used without Tris–HCl buffer solution for all experiments [16].

2.2. Characterization

2.2.1. Wide-Angle X-ray Diffraction (WAXD)

WAXD analyses were performed for the SAN powder and nanocomposite hydrogels using an Mxlabo X-ray diffractometer (MAC Science Co. 3 kW, graphite monochromator, Cu Kα radiation ($\lambda_x = 0.154$ nm), operated at 40 kV and 20 mA). Samples were scanned in fixed time mode with counting time of 2 s at room temperature under diffraction angle 2θ in the range of 1–30°.

2.2.2. Fourier Transform Infrared Spectroscopy (FTIR)

FTIR spectra were collected at 1 cm^{-1} nominal resolution using a FTIR spectrometer (FT-730, Horiba Ltd.) equipped with ZnSe mull omni-cell window (GS01834, Specac Co. UK) in transmission mode. The spectra were obtained by averaging 32 scans with a mean collection length of 1 s per spectrum. The background spectra used for reduction were collected with sample. By subtracting the spectrum of SWN/water from the consecutive spectra, a difference spectrum was processed by software.

2.2.3. Rheology

Rheological measurements were also conducted on RDAII instrument with a torque transducer capable of measurements over the range of 0.2–200 g cm. Dynamic oscillatory shear measurements were performed by applying a time dependent strain of $\gamma(t) = \gamma_o \sin(\omega t)$, where γ_o is the strain amplitude, ω is the frequency, and t is the time. The resultant shear stress is $\sigma(t) = \gamma_o [G'\sin(\omega t) + G''\cos(\omega t)]$, with G' and G'' being the storage and loss modulus, respectively. Measurements were conducted by using a cone-plate geometry of cone angle of 0.1 rad and diameter of 25.0 mm operated at 25 °C. To check the nonlinear response, the dynamic strain sweep test was conducted at the strain amplitude range of 0.005–0.1 at fixed frequency of 1.0 rad s^{-1}.

Stress relaxation measurements were performed at 25 °C using a set of 25 mm diameter parallel plates. A single step strain γ was applied at time $t = 0$, and the shear stress $\sigma(t)$ was measured as a function of time, with the modulus $G(t, \gamma)$ obtained as $G(t, \gamma) = \sigma(t)/\gamma$. The stress relaxation data were obtained at $\gamma = 0.003–0.03$. At low strain ($\gamma = 0.003–0.01$), the data were verified to be in the linear regime.

3. Results and discussion

3.1. WAXD patterns of nanocomposite hydrogels

WAXD offers a convenient method to determine the interlayer spacing of the clay layers in the original clay and in the intercalated structure in the nanocomposite hydrogels. WAXD patterns for SWN powder and the nanocomposite hydrogels with different concentration ($\phi_{SWN} = 0.016–0.101$) are presented in Fig. 1. The mean basal spacing of the (001) plane ($d_{(001)}$) for SWN powder obtained by WAXD measurements is 1.29 nm ($2\theta \cong 6.81°$) (indicating by dashed line in figure) (Fig. 1a). For SWN hydrogels without DNA, a clear peak is obtained at $2\theta \cong 5.0°$ for the hydrogel with $\phi_{SWN} = 0.016$. With increasing SWN content, this peak shifted toward the higher diffraction angle at $2\theta \cong 5.5°$, whereas for nanocomposite hydrogels with DNA the peak shift exhibits opposite trend (Fig. 1b).

Fig. 2 representd the SWN content (ϕ_{SWN}) dependent $d_{(001)}$ and the number of the staked individual silicate layers ($=(D/d_{(001)}) + 1$) of nanocomposite hydrogels. The crystallite size (D) of intercalated-and-stacked silicate layers of the dispersed SWN in hydrogels was calculated by using the Scherrer equation [17]. The presence of 2 wt% DNA

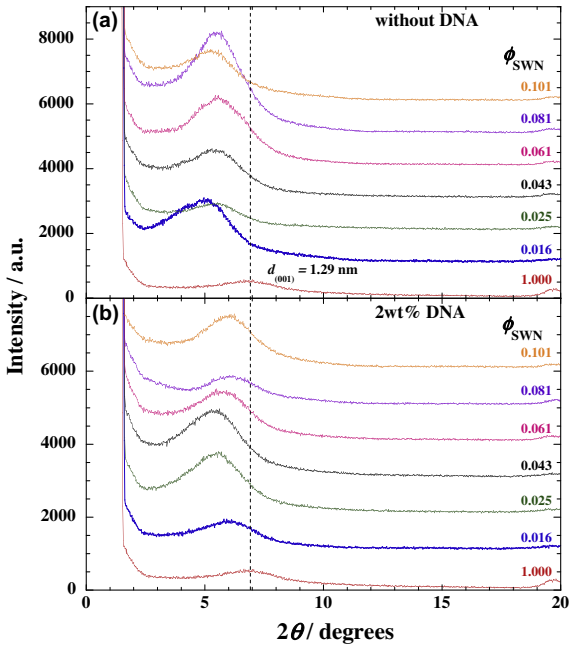

Fig. 1. WAXD patterns for (a) SWN hydrogels and (b) DNA/SWN nanocomposite hydrogels SAN with different concentration (ϕ_{SWN} = 0.016–0.101). The dashed line indicates the location of the silicate (001) reflection of SWN powder. The data on *Y*-axis were shifted to avoid overlapping.

does not lead to a significant shift in basal spacing and stacked structure of the dispersed SWN as compared with SWN hydrogels without DNA. We confirmed that this behavior is intrinsic hydrophilic nature, which is presumably ascribed to the intercalation of water molecules into the silicate galleries and coherent order of the silicate layers is much higher in hydrogel as compared with powder form of SWN. The interlayer distance is 0.68 nm, which is estimated by subtracting the value of layer thichness (0.92 nm) of smectite [18]. Avinash et al. [19] reported the molecular dimension of intact double-stranded DNA intercalated into nano-galleries of organically modified clay. Since the width of the double-stranded DNA is almost 2 nm by considering the value of the expansion of $d_{(001)}$, the interlayer distance of 0.68 nm does not allow the intercalation of DNA macromolecules into SWN nano-galleries.

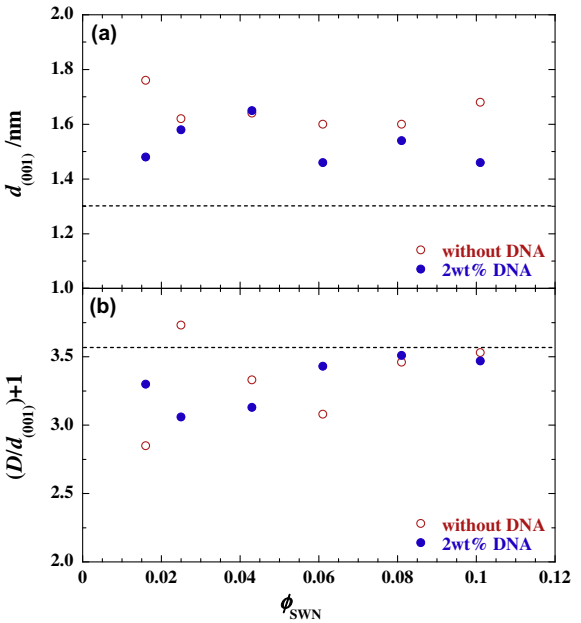

Fig. 2. SWN content (ϕ_{SWN}) dependent (a) $d_{(001)}$ and (b) the number of the staked individual silicate layers (=$(D/d_{(001)})$ + 1) of hydrogels.

3.2. FTIR spectra of nanocomposite hydrogels

The frequencies and the vibrational assignments for the DNA with B-form and clay minerals are reported in the literature. Fig. 3a shows the spectral variations of SWN hydrogel (ϕ_{SWN} = 0.043) in the region of 1800–800 cm^{-1}. A band located at 3450 cm^{-1} (data not shown) is assigned to the OH stretching mode (ν(OH)), and the band at 1650 cm^{-1} is due to the hydroxyl bending vibration (δ(OH)) from water. The characteristic Si—O bands are observed at 1080 cm^{-1} (out-of-plane ν(Si—O)) and 1000 cm^{-1}

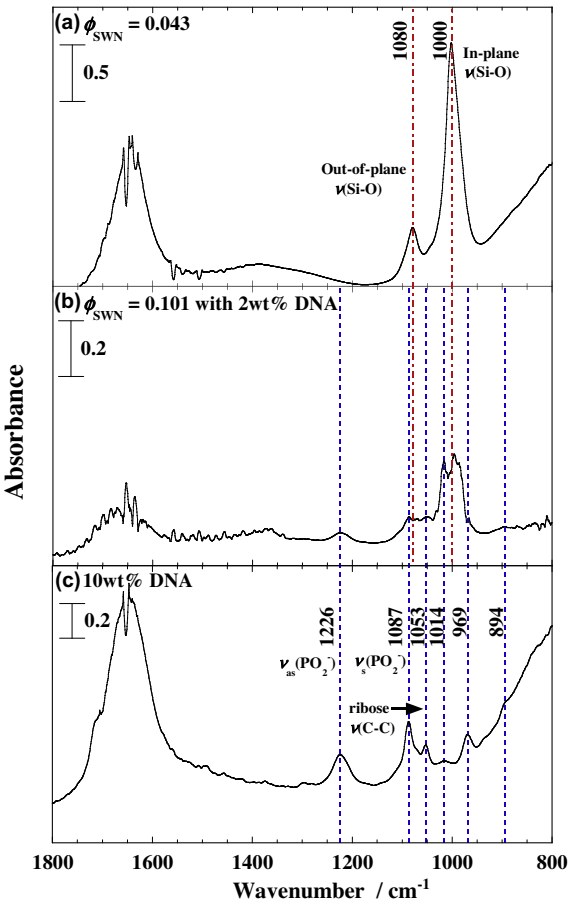

Fig. 3. FTIR spectra of (a) SWN hydrogel with ϕ_{SWN} = 0.043, (b) difference spectra of DNA/SWN hydrogel with ϕ_{SWN} = 0.101 and (c) 10 wt% DNA aqueous solution in the region of 800–1800 cm^{-1}.

(in-plane ν(Si—O)) [20]. These sensitive bands appear when the clay particles are dispersed in water [21]. The band at 1080 cm^{-1} shifs to lower frequency in the hydrogel, reflecting the formation of the intermolecular hydrogen bonding between Si–OH groups on the edge surface of SWN and H_2O molecules.

In Fig. 3c, bands located in the region of 1750–1600 cm^{-1}, which are common to C═O, C═N, C═C stretching and exocyclic —NH_2 bending vibrations in the DNA bases [22]. The sensitive bands at 1226 cm^{-1} (asymmetric stretching mode of PO_2^- groups: $\nu_{as}(PO_2^-)$), 1087 cm^{-1} (symmetric stretching mode: $\nu_s(PO_2^-)$) and 1053 cm^{-1} (stretching of ribose ν(C—C)) of the phosphodiester–deoxyribose backbone provide valuable information to understand the interaction generated between DNA backbone and SWN surfaces. The B-form DNA shows characteristic absorbance peaks at 1014 (double-stranded DNA in B-form), 969 and 894 cm^{-1} as seen in the region from 850 to 1050 cm^{-1}.

By subtracting the spectrum of SWN hydrogel from the consecutive spectra of nanocomposite hydrogel with 2 wt% DNA, a difference spectrum was obtained (Fig. 3b). The presence of the sensitive bands in the difference spectrum is also confirmed. Fig. 4 shows the typical example of ϕ_{SWN} dependence of frequency shift for the characteristic bands. We notice that $\nu_{as}(PO_2^-)$ band shifts to the lower frequency side with increasing of SWN concentration. In contrast, the variation of $\nu_s(PO_2^-)$ exhibits nearly constant. The formation of the interaction between PO_2^- groups of DNA and SWN surfaces was speculated. However, the structural change of the DNA backbone does not take place because the characteristic bands of B-form DNA are not disappeared as seen in Fig. 3b. The weak frequency shift to the lower side in out-of-plane Si–O bonds accompanied with almost constant frequency for in-plane Si–O bonds is presumably due to the different degree of the delamination of the dispersed SWN particles in water. This feature also observed in SWN hydrogels with different ϕ_{SWN}.

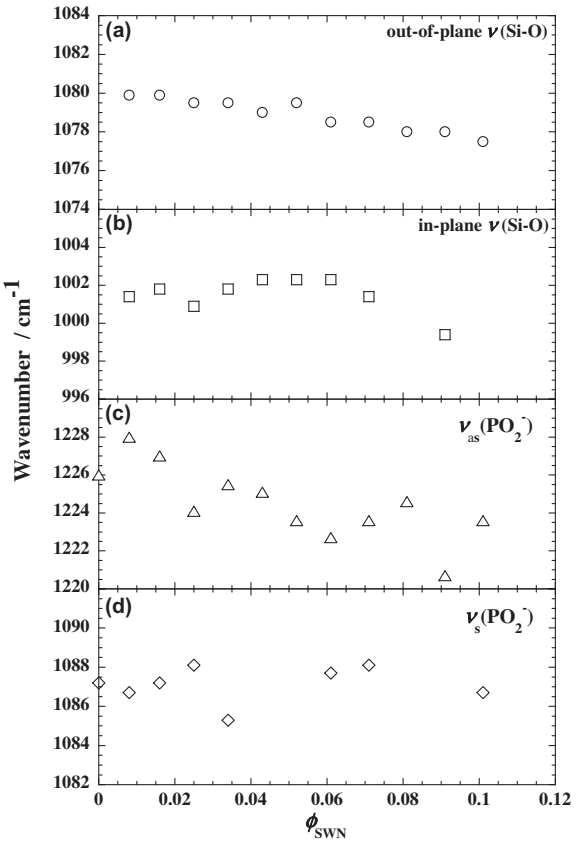

Fig. 4. ϕ_{SWN} dependence of frequency shift for the characteristic bands: (a) out-of-plane ν(Si—O), (b) in-plane ν(Si—O), (c) asymmetric stretching mode of PO_2^- groups: $\nu_{as}(PO_2^-)$ and (d) symmetric stretching mode: $\nu_s(PO_2^-)$.

3.3. Solid-like Rheology

The central discussion in DNA/SWN nanocomposite hydrogels is the structure with elasticity. Fig. 5 shows the typical frequency ω dependence linear viscoelasticity. We can clearly see that both moduli are almost independent of ω with the exception of decreasing of $G'(\omega)$ at low region ($\omega < 1$ rad/s). The value of $G'(\omega)$ is larger than that of $G''(\omega)$ within a flame work of ω, suggesting the system is a viscoelastic solid-like hydrogel (Fig. 5a and c). Furthermore, the increment of both moduli with increasing ϕ_{SWN} evolves by order of magnitude. At the long relaxation time end ($\omega \sim 0.03$ rad/s), the plateau $G''(\omega)$ exhibits large increasing in viscosity ($\cong G''(\omega)/\omega$) for the hydrogels with ϕ_{SWN} = 0.016–0.025. This tendency resembles the relaxation of the internal developed structure as described later.

For DNA/SWN nanocomposite hydrogels, the tendency is almost the same as for SWN hydrogels. An interesting aspect of the solid-like hydrogel is the significant drop in $G'(\omega)$ as compared with SWN hydrogels without DNA (Fig. 5b). At the same time, the enhancement in $G''(\omega)$ seems to stem from the damping effect of the dispersed SWN particles (Fig. 5d). We can speculate this behavior comes from the softening of the hydrogels due to the incorporation of DNA molecules (see stress of the hydrogel at break: σ_{break} in Fig. 8).

The dynamic complex viscosity ($|\eta^*|(\omega)$) curves for each system, based on linear dynamic oscillatory shear measurements are conducted (Fig. 6). We observed very strong shear-thinning tendency in the rapid shear flow in each system. The complex viscosity is enhanced considerably at all shear rates, and increases monotonically with increasing ϕ_{SWN}. In our previous study [23] on lipophilized-hectorite/toluene suspensions, we observed this type of shear-thinning feature of the clay particles in the rapid shear flow. The possible reason of this behavior may be due to the planer alignment of the SWN particles towards the flow direction under shear. This feature is strongly dependent on the shear rate and strain in the measurements because of the formation of the shear-induced alignment of the dispersed SWN particles [24].

3.4. Mesoscale structure development

Since frequency dependent viscosity of each hydrogel nicely show non-Newtonian behavior, therefore Casson relation [25] is applicable for all systems. Fig. 7 represents

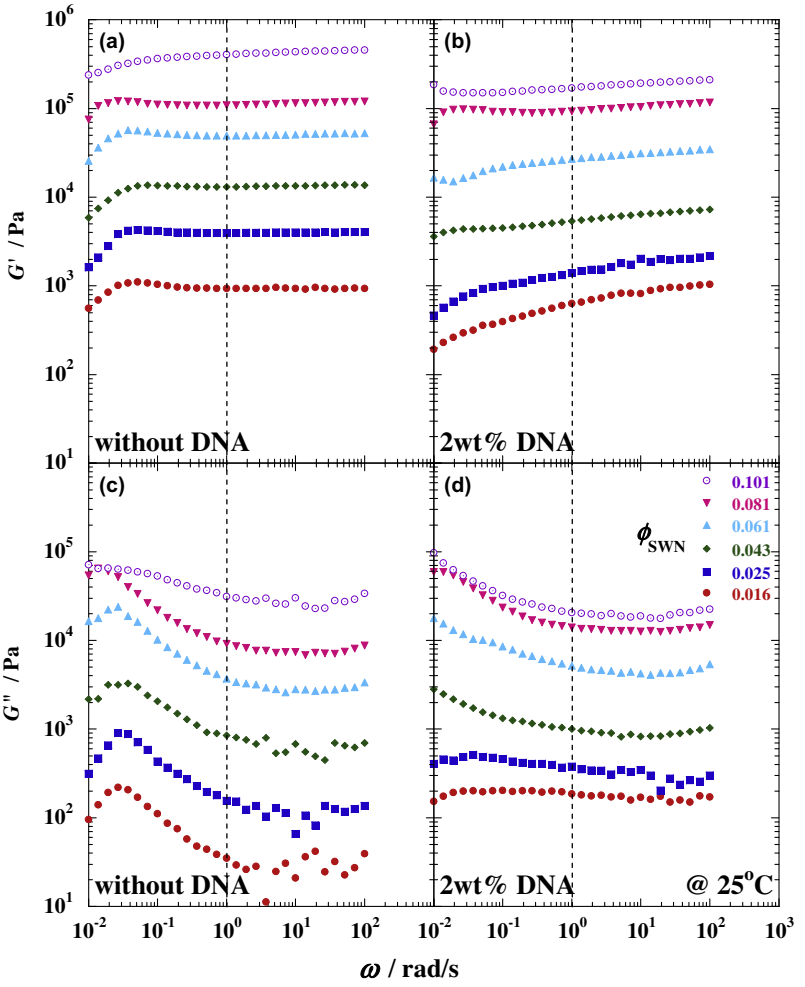

Fig. 5. Frequency ω dependence of (a, b) storage modulus $G'(\omega)$ and (c, d) loss modulus $G''(\omega)$ for SWN and DNA/SWN hydrogels. The dashed line indicates the location of ω = 1.0 rad/s.

the Casson plot for two sets of DNA/SWN and SWN hydrogels with ϕ_{SWN} = 0.025 and 0.101, and intercept (k_0) of this plot give us stress of these hydrogel at break i.e., σ_{break}. In Fig. 8, we show double logarithmic plot of ϕ_{SWN} dependence of σ_{break} of various DNA/SWN and SWN hydrogels. σ_{break} systematically increases with increasing SWN content in each system. This behavior is strongly related with the strong flocculation of the H_2O intercalated SWN layers dispersed in water medium. In this region, the power law relation for ω limiting value of complex modulus G^* (ω = 1.0 rad/s, marked with dashed line in Fig. 5) was obtained as follows:

$$G^* \sim \sigma_{break} \sim \phi_{SWN}^{\alpha} \quad (1)$$

Interestingly, the obtained exponent α of 4.0 is higher value than that of about 3 reported value by Ramsay [26]. Furthermore, all systems examined the plots nicely conform to straight lines in both characteristic parameters (i.e., G^* and σ_{break}) regardless of the probe. Presumably these systems are strongly flocculated compared to the Ramsay's aqueous suspension system.

3.5. Stress-relaxation of hydrogels

The stress-relaxation behaviors of DNA/SWN and SWN hydrogels in the linear viscoelastic regime (γ < 0.02 for SWN hydrogel and γ < 0.01 for DNA/SWN nanocomposite hydrogel, respectively) and non-linear viscoelastic regime are presented in Fig. 9. The adopted strain amplitudes, 0.02 and 0.01 for the hydrogel with ϕ_{SWN} = 0.101, are shown in Fig. 10. Within the testing strain range from 0.003 to 0.03, the stress is linearly increased with strain amplitude, therefore the magnitude of stress at large strain (non-linear regime) is larger than that at small strain (linear regime).

The shear relaxation modulus $G(t, \gamma)$ can be factored into a linear relaxation modulus $G(t)$ and strain-dependency function, often called damping function $h(\gamma)$, in the long-time region, which is given by [27]

$$G(t, \gamma) = G(t)h(\gamma) \quad (2)$$

In Fig. 9, the vertical axis is reduced by $h(\gamma)$ because of the discussion in the damping effect of the dispersed SWN particles in the DNA/SWN nanocomposite hydrogel. For

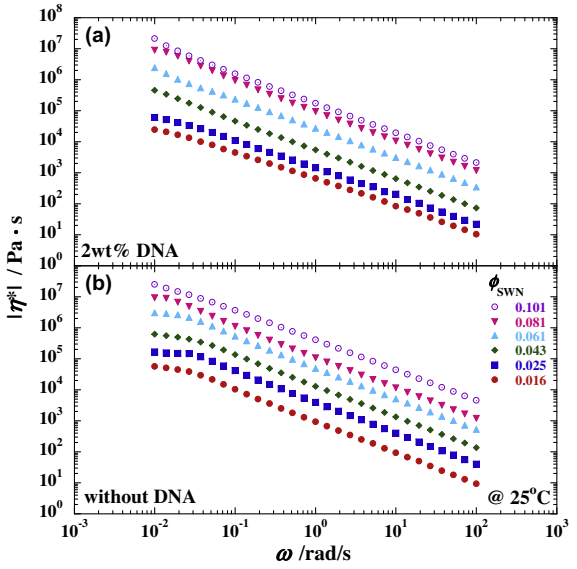

Fig. 6. Frequency ω dependence of complex viscosity ($|\eta^*|(\omega)$) of SWN and DNA/SWN hydrogels with different concentration (ϕ_{SWN} = 0.016–0.101).

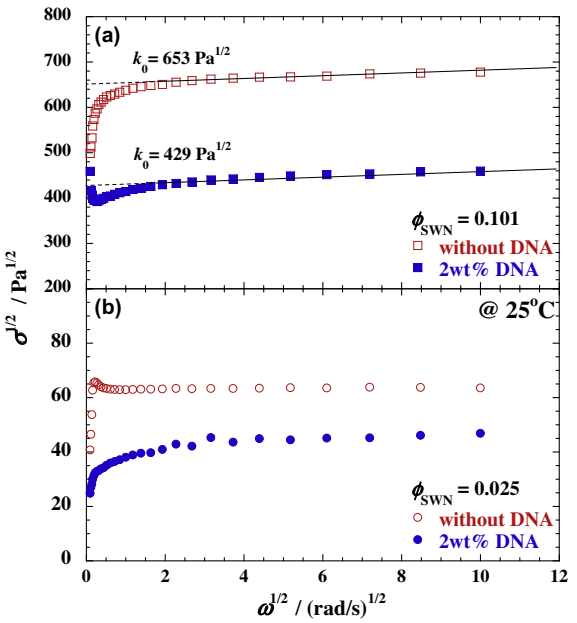

Fig. 7. Casson plot for two sets of SWN and DNA/SWN hydrogels with (a) ϕ_{SWN} = 0.101 and (b) 0.025. The dashed lines indicate the intercept of the plots.

SWN hydrogel, the stress decreases with time and the relaxation behavior is similar for all imposed strain. At long time, however, DNA/SWN hydrogel relaxes like a liquid at small strains (γ = 0.003–0.007), while the system behaves like a solid-like gel for times as long as 1000 s in excess of γ = 0.07.

The damping function is plotted as a function of strain for DNA/SWN and SWN hydrogels with ϕ_{SWN} = 0.101. It is

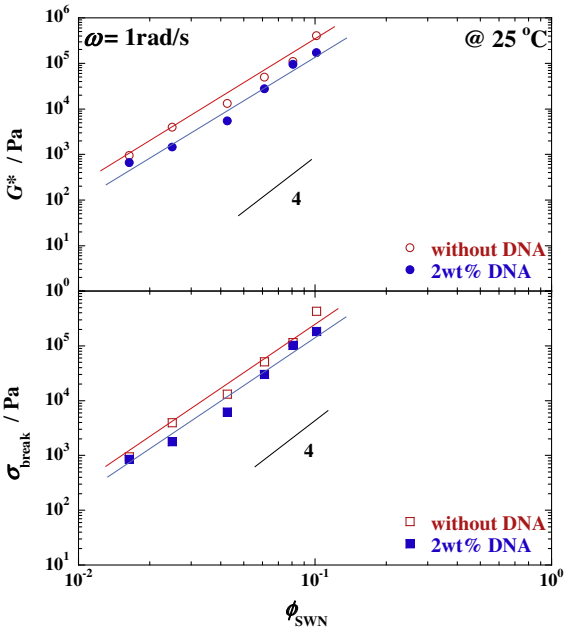

Fig. 8. Double logarithmic plot of ϕ_{SWN} dependence of G^* and σ_{break} for various DNA/SWN and SWN hydrogels.

obvious that, with increasing strain, the deviation (strain softening) increases in DNA/SWN nanocomposite hydrogel. The damping function of Fig. 11 can be fit out to a strain by a simple exponential equation given by [28]

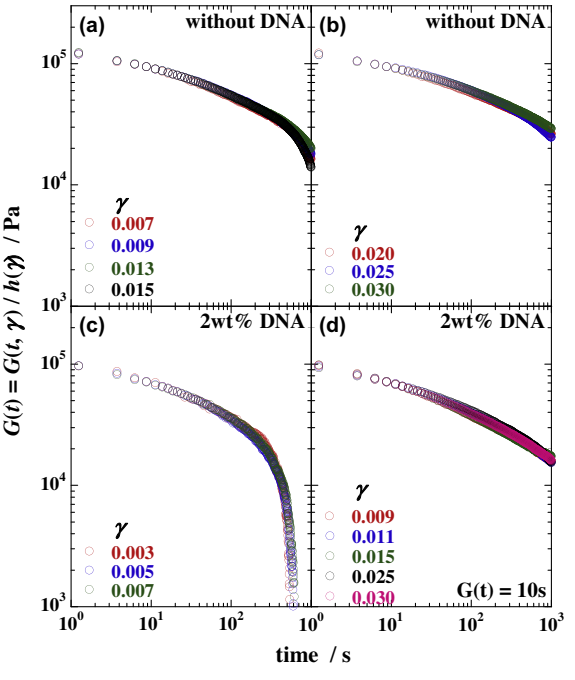

Fig. 9. Reduced stress-relaxation spectra of DNA/SWN and SWN hydrogels in (a, c) linear viscoelastic regime and (b, d) non-linear viscoelastic regime.

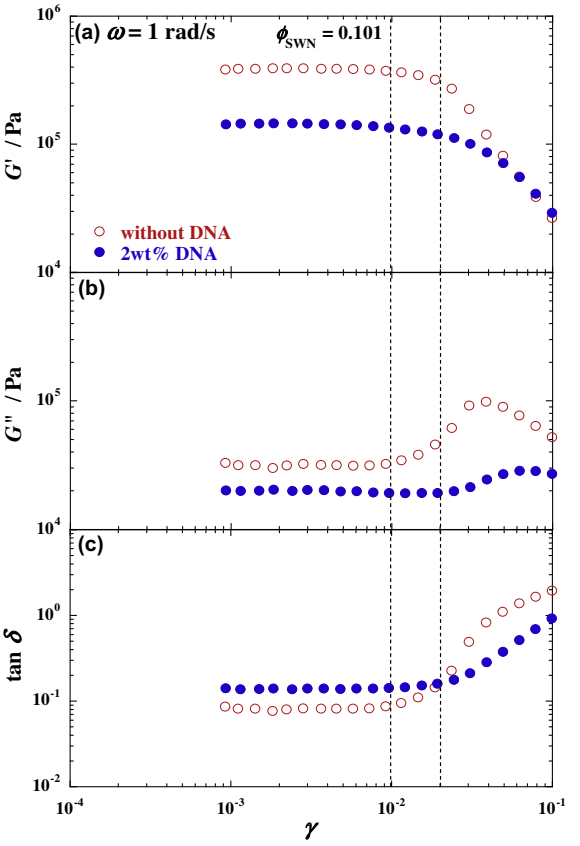

Fig. 10. (a) Storage modulus $G'(\omega)$, (b) loss modulus $G''(\omega)$ and (c) tan δ versus strain. The dashed lines indicates the location of the adopted strain amplitudes for the terminal strain of linear viscoelastic regime ($\gamma = 0.01$ for DNA/SWN and 0.02 for SWN hydrogels, respectively).

$$h(\gamma) = c_1 \exp(-a\gamma) \tag{3}$$

The parameters c_1 and a in each system are presented in Table 1. The experimental results can be fit fairly well by the simple expression. The parameter a in DNA/SWN hydrogel exhibits a one order of magnitude higher than the value of SWN hydrogel, suggesting the softening of the nanocomposite hydrogel as discussed above.

The stress relaxation modulus is related to the relaxation spectrum ($H(\lambda)$) as [29]

$$G(t) = \int_{-\infty}^{\infty} H(\lambda) \exp(-t/\lambda) d \ln \lambda \tag{4}$$

Using it provides a continuous function of the relaxation time (λ) rather than a discrete set. On the basis of the dynamic relaxation response shown in Fig. 9 and using Eq. (4), the relaxation spectrum was calculated and is shown in Fig. 12. Beyond $\lambda = 100$ s, $H(\lambda)$ of the nanocomposite hydrogel in the linear regime ($\gamma = 0.007$) suddenly decreases with a very large value of 10^4 Pa, suggesting the lack of the component for longest relaxation time in the system. On the other hand, the relaxation spectrum of DNA/SWN hydrogel in the non-linear regime ($\gamma = 0.030$) are comparable to that of SWN hydrogel. The agreement between the measured $G(t, \gamma)$ (Fig. 9) and the calculated value of $H(\lambda)$ (Fig. 12) is excellent. The liquid-like relaxation observed for DNA/SWN hydrogel at small strain changes to solid-like behavior in excess of $\gamma = 0.07$. We discuss these features in the following section.

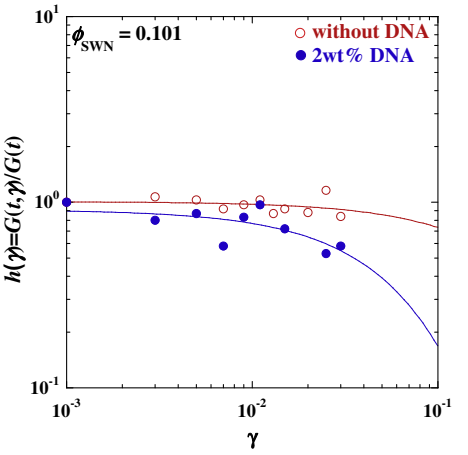

Fig. 11. Damping function of SWN and DNA/SWN hydrogels with $\phi_{SWN} = 0.101$. The solid curves represent the fits by Eq. (3).

Table 1
Parameters c_1 and a obtained from simple exponential Eq. (3).

Hydrogels	c_1	a
SWN	1.01	0.03
DNA/SWN	0.91	0.17

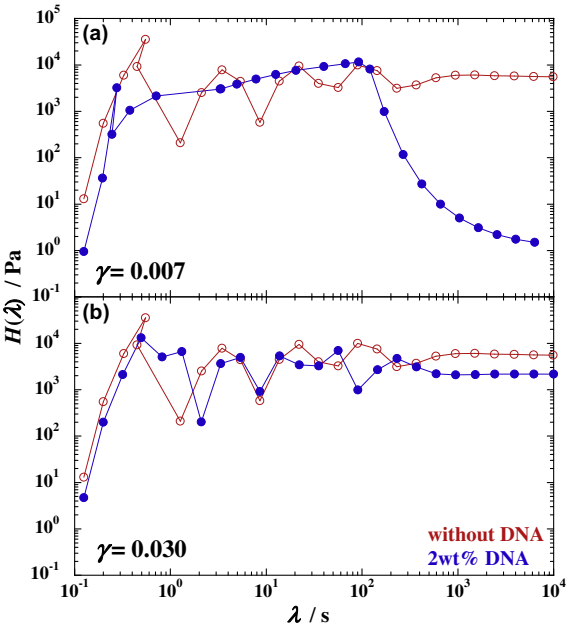

Fig. 12. Relaxation spectra of (a) in linear viscoelastic regime ($\gamma = 0.007$) and (b) in non-linear viscoelastic regime ($\gamma = 0.030$) for DNA/SWN and SWN hydrogels.

3.6. Network formation and rupture

An important question is how long the build of the solid-like network structure continues during flow, i.e., reversibility of the network formation process. By imposing the constant shear strain, the deflocculation and/or flocculation of the structure may occur as revealed by the stress-relaxation with time. Under non-linear regime, the relaxation spectra of DNA/SWN and SWN hydrogels are almost identical. The stress relaxation behavior imposed a small strain offers insight into mesoscale network structural changes. The structure disorder creates energy barriers that prevent reorganization/reconstituting of networks into states of lower free energy. In dynamics for a typical soft glassy material, slow degree of freedom is taken into account [12,30]. The jamming is a common property of the complex fluids. In the presence of strain, the stress is given by the distribution of relaxation times of "slow mode" in the networks.

Imposition of shear is considered to change the energy landscape and allows for the system to access new metastable states [31]. For this reason, the imposition of weak deformation (γ = 0.003–0.007) (much smaller than yield strain: see Fig. 10) is considered as shear deflocculation condition, meaning that the longest relaxation time of the slow mode decreases in time. The rupture of the initial network structure takes place and a steady state without long-range gelation is finally reached.

In the case of large deformation (γ = 0.009–0.030), those energy barriers become greater the longer a system is aged such that the longest relaxation time continuously remains at constant values. Therefore, the network may become trapped in a higher energy state due to the formation of the shear-induced alignment of the dispersed SWN particles in the hydrogel. Brownian forces alone are unable to change the energy barriers created by such oriented network structure. Such discussion on energy landscape appears to be entirely valid for the experimental results as well as polymer/clay nanocomposite melts [32].

4. Conclusions

We have successfully prepared DNA-based nanocomposite hydrogels with different SWN content. The mesoscale structure of the nanocomposite hydrogels was directly related to the hydrophilic nature of SWN and also DNA macromolecules. The intercalation of water molecules into the silicate galleries took place and the interaction between PO_2^- groups of DNA and SWN surfaces without the structural change of the DNA backbone was speculated as revealed by WAXD and FTIR analyses. DNA/SWN hydrogels exhibited viscoelastic solid-like properties. However, the incorporation of DNA macromolecules led to the enhancement of the damping behavior of the dispersed silicate particles as compared with SWN hydrogels without DNA. The softening of the nanocomposite hydrogels was also supported by the calculated damping function of the stress-relaxation measurements. We have observed very interesting features in the relaxation spectra between linear and non-linear regimes. Under linear regime, the liquid-like relaxation observed for DNA/SWN hydrogel suddenly changed to solid-like behavior in excess of γ = 0.07. The imposition of weak deformation in DNA/SWN hydrogel was considered as shear deflocculation condition, where the initial network structure was ruptured accompanied with the lack of the longest relaxation time.

Acknowledgments

This work was supported by KAKENHI (22656148) and the Strategic Research Infrastructure Project of the Ministry of Education, Sports, Science and Technology, Japan (2010-2014).

References

[1] Sinha Ray S, Okamoto M. Polymer/layered silicate nanocomposites: a review from preparation to processing. Prog Polym Sci 2003;28:1539–641.
[2] Vaia RA, Wagner HD. Framework for nanocomposites. Mater Today 2004;7:32–7.
[3] Gao F. Clay/polymer composites: the story. Mater Today 2004;7:50–5.
[4] Okamoto M. Recent advances in polymer/layered silicate nanocomposites: an overview from science to technology. Mater Sci Technol 2006;22:756–79.
[5] Okada A, Usuki A. Twenty years of polymer-clay nanocomposites. Macromol Mater Eng 2006;291:1449–76.
[6] Hussain F, Hojjati M, Okamoto M, Gorga RE. Review paper: polymer–matrix nanocomposites, processing, manufacturing, and application: an overview. J Compos Mater 2006;40:1511–75.
[7] Usuki A, Kojima Y, Okada A, Fukushima Y, Kurauchi T, Kamigaito O. Swelling behavior of montmorillonite cation exchanged for ω-amino acids by ε-caprolactam. J Mater Res 1993;8:1174–8.
[8] Vaia RA, Giannelis EP. Polymer melt intercalation in organically-modified layered silicates: model predictions and experiment. Macromolecules 1997;30:8000–9.
[9] Krishnamoorti R, Vaia RA, Giannelis EP. Structure and dynamics of polymer-layered silicate nanocomposites. Chem Mater 1996;8:1728–34.
[10] Rao Y, Pochan JM. Mechanics of polymer–clay nanocomposites. Macromolecules 2007;40:290–6.
[11] Treece MA, Oberhauser JP. Soft glassy dynamics in polypropylene-clay nanocomposites. Macromolecules 2007;40:571–82.
[12] Sollich P, Lequeux F, Hebraud P, Cate ME. Rheology of soft glassy materials. Phys Rev Lett 1997;78:2020–3.
[13] Haraguchi K, Takeshita T. Nanocomposite hydrogels: a unique organic–inorganic network structure with extraordinary mechanical, optical, and swelling/de-swelling properties. Adv Mater 2002;14:1121–4.
[14] Haraguchi K, Takeshita T, Fan S. Effects of clay content on the properties of nanocomposite hydrogels composed of poly(N-isopropylacrylamide) and clay. Macromolecules 2002;35:10162–71.
[15] van Olphen H. An introduction to clay colloid chemistry. New York: Wiley; 1977.
[16] Ruiz-hitzky E, Ariga K, Lvov Y, editors. Bio-inorganic hybrid nanomaterials. Wiley-VCH; 2008.
[17] Sinha Ray S, Yamada K, Okamoto M, Ogami A, Ueda K. New polylactide/layered silicate nanocomposites. 3. high-performance biodegradable materials. Chem Mater 2003;15:1456–65.
[18] Heinz H, vaia RA, Krishnamoorti R, Farmer BI. Self-assembly of alkylammonium chains on montmorillonite: effect of chain length, head group structure, and cation exchange capacity. Chem Mater 2007;19:59–68.
[19] Avinash JP, Mei L, Erik D, Stephen M. Novel bioinorganic nanostructures based on mesolamellar intercalation or single-molecule wrapping of DNA Using organoclay building blocks. Nano Lett 2007;7:2660–5.
[20] Marel HMV, Bentelspacher H. Atras of infrared spectroscopy of clay minerals and their admixtures. New York: Elsevier; 1976.
[21] Ijdo WL, Kemnetz S, Benderly D. An infrared method to assess organoclay delamnination and orientation in organoclay polymer nanocomposites. Polym Eng Sci 2006;46. 1301–1039.
[22] Brewer SH, Annthireya SJ, Lappi SE, Drapcho DL, Franzen S. Detection of DNA hybridization on gold surfaces by polarization modulation

infrared reflection absorption spectroscopy. Langmuir 2002;18:4460–4.
[23] Okamoto M, Taguchi H, Sato H, Sato H, Kotaka T, Tateyama H. Dispersed structure and Rheology of lipophilized-smectite/toluene suspensions. Langmuir 2000;16:4055–8.
[24] Okamoto M, Nam PH, Maiti P, Kotaka T, Hasegawa N, Usuki A. A house of cards structure in polypropylene/clay nanocomposites under elongational flow. Nano Lett 2001;1:295–8.
[25] Utracki LA. Polymer alloya and blends: thermodynamics and Rheology. New York: Hasser Publishers; 1990.
[26] Ramsay JDF. Colloidal properties of synthetic hectorite clay dispersions: I Rheology. J Colloid Interf Sci 1986;109:441–7.
[27] Doi M, Edwards SF. The theory of polymer dynamics. Oxford, UK: Oxford University Press; 1986.
[28] Wagner MH. Analysis of time-dependent non-linear stress-growth data for shear and elongational flow of a low-density branched polyethylene melt. Rheol Acta 1976;15:136–42.
[29] Ferry JD. Viscoelastic properties of polymers. New York: John Wiley & Sons; 1980.
[30] Bonn D, Tanase S, Abou B, Tanaka H, Meunier J. Laponite: aging and shear rejuvenation of a colloidal glass. Phys Rev Lett 2002;89:015701.
[31] Gagnon G, Patton J, Lacks DJ. Energy landscape view of fracture and avalanches in disordered materials. Phys Rev E 2001;64:51508.
[32] Katoh Y, Okamoto M. Crystallization controlled by layered silicates in nylon 6-clay nano-composite. Polymer 2009;50:4718–26.